**Proceedings of the ASME 2018
Conference on Smart Materials, Adaptive Structures and Intelligent Systems
SMASIS2018
September 10-12, 2018, San Antonio, TX, USA**

SMASIS2018-8127

PIEZOELECTRIC VIBRATION CONTROL OF A SANDWICH BEAM WITH TIP MASS

Eshagh Farzaneh
Mechanical Engineering
Central Michigan University
Mt Pleasant, MI, USA

Oumar Barry
Mechanical Engineering
Virginia Polytechnic Institute and State University
Blacksburg, VA, USA

Pablo Tarazaga
Mechanical Engineering
Virginia Polytechnic Institute and State University
Blacksburg, VA, USA

ABSTRACT

This paper studies the vibration mitigation of a sandwich beam with tip mass using piezoelectric active control. The core of the sandwich beam is made of foam and the face sheets are made of steel with a bonded piezoelectric actuator and sensor. The three-layer sandwich beam is clamped at one end and carries a payload at the other end. The tip mass is such that its center of mass is offset from the point of attachment. The extended higher-order sandwich panel (HSAPT) theory is employed in conjunction with the Hamilton's principle to derive the governing equations of motion and boundary conditions. The obtained partial differential equations are solved using the generalized differential quadrature (GDQ) method. Free and forced vibration analyses are carried out and the results are compared with those obtained from the use of the commercial finite element software ANSYS. Derivative feedback control algorithm is employed to control the vibration of the system. Parametric studies are conducted to examine the arrangement impact of the piezoelectric sensors and actuators on the system vibrational behavior.

INTRODUCTION

Most engineering structures and devices are prone to unwanted vibrations induced by environment conditions. When left uncontrolled, these vibrations can cause fatigue failures and eventually undermining public safety and/or resulting in significant economic loss. The control of these vibrations can be achieved through passive, active, or semi-active techniques. Passive isolation offer a simple, cost-effective, reliable, and energy efficient means of vibration isolation, but they are only effective within a limited range of excitation frequency [1, 2]. Active vibration control involves the use of sensors and actuators in a system to measure the structural response and produce control forces to eliminate the vibration of the host structure [3]. Semi-active isolation is a combination of passive devices with controllable properties [4].

When higher performance is desired, active vibration control is the best choice among the three aforementioned isolation techniques. Recently, piezoelectric smart structures have been widely employed for active vibration control applications [5]-[20]. These smart structures are usually very flexible and can consist of regular or sandwich beams or plates bounded with piezoelectric patches [20]. In aerospace applications, sandwich structures are among the most commonly used flexible members because of their high specific stiffness, high specific strength, low structural weight, and high absorption capability. A typical sandwich structure comprises two outer layers (or face sheets) of identical geometric and material properties and one middle layer (or core). When vibration suppression is the primary goal, the core is softer than the face sheets. However, the use of soft material in the core of sandwich structures call for the relaxation of a constant core transverse displacement, which cannot be properly handled with classical models based on the first order shear deformation theory (FOSDT).

Modern models based on high order sandwich panel theory (HSAPT) are proposed [21, 22, 23, 24, 25, 26] to accurately predict the dynamic of soft core sandwich structures. The original HSAPT model used mixed formulation in which the unknown generalized displacement variables are the axial and transverse displacements of the top and bottom face sheets, and the uniform shear stress in the core [23]. Other HSAPT models replace the core shear stress variable by the mid-core transverse displacement. Such models are called HSAPT displacement [24]. The most modern model of sandwich structures is the extended high order sandwich panel (EHSAPT), which is an improvement of the HSAPT and is applicable to both soft and hard-core sandwich structures. EHSAPT incorporates the in-plane core rigidity and extends the HSAPT generalized displacement variables by including the axial and transverse displacements and the rotation at the centroid of the core [27].

Regarding control algorithms for vibration suppression in smart composite structures, numerous techniques have been proposed in the literature. This includes the linear quadratic regulator (LQR) [28], velocity feedback control [28, 29, 30], and proportional-integral-derivative (PID) control [31]. It should be noted that direct velocity feedback and PID are the most commonly used piezoelectric vibration control due to their simplest design and implementation [32].

The direct velocity feedback control is adopted in this paper to control the vibration of a sandwich beam with tip mass. It is worth noting that the majority of previous works focus on controlling bare sandwich beams. To our best knowledge, there is no work in the literature that studies the piezoelectric vibration control of a sandwich beam with tip mass. The investigation of this problem is reported in this paper for the first time. The tip mass of the sandwich beam is such that its center of gravity is offset from the point of attachment. The core of the sandwich beam is made of foam and the face sheets are made of steel. The HSAPT and Hamilton's principle are used in deriving the governing equations of motion and boundary conditions. Natural frequencies and vibration response of the system are obtained using the GDQ method and the results are compared to those of ANSYS. Parametric studies are carried out to examine the role of sensor and actuator location on the performance of the controller.

MATHEMATICAL MODELING

A schematic diagram of the sandwich beam with tip mass along with attached piezoelectric patches is shown in Fig.1. The length and the width of the beam are L and b respectively. This beam is composed of three layers. Two thin/stiff face sheets with thickness h_f and a thick/soft core with a thickness h_c. The length of the tip mass is defined as L_M. The length, thickness, and width of the piezoelectric patches are $L_p, h_p,$ and b, respectively.

As it can be seen from Fig. 2, the piezoelectric patches considered here act as sensors and actuators. The electrical potential of the sensor is defined as ψ_s and that of the actuator is defined as ψ_a. It is assumed that the piezoelectric layers and the face sheets deform according to the Euler-Bernoulli beam theory.

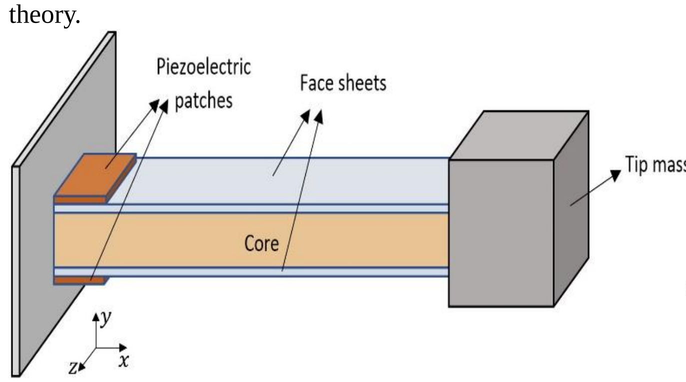

Figure 1. Schematic of sandwich beam with tip mass attached with piezoelectric patches.

This assumption is reasonable as the face sheets and piezoelectric layers are very thin and only change in the length. The core, however, is thick and consequently it can change in both length and thickness. To this end, the displacement fields of the core are based on the HSAPT to account for its in-plane rigidity along with its flexibility in the transverse direction.

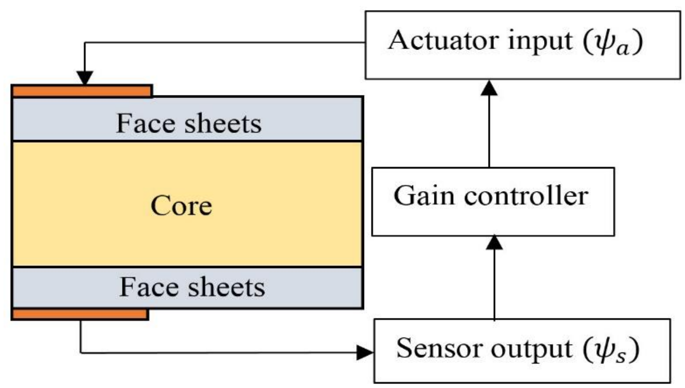

Figure 2. Sensor and actuator and feedback control loop.

The total kinetic (T) and potential (U) energies of the system depicted in Fig.1 are given as:

$$T = T_{beam} + T_{tip\ mass} + T_{piezo}$$
$$U = U_{beam} + U_{piezo} \tag{1}$$

The kinetic energy of the beam is

$$T_{beam} = \frac{1}{2}\int \rho_f[(\dot{u}_t - y\dot{w}_t')^2 + \dot{w}_t^2]\, dV_t + \frac{1}{2}\int \rho_f[(\dot{u}_b - y\dot{w}_b')^2 + \dot{w}_b^2] dV_b + \frac{1}{2}\int \rho_c \left[\left(\dot{u}_c + \dot{\phi}_1 y + \left(\dot{u}_t + \dot{u}_b + \frac{h_f}{2}\dot{w}_t' - \frac{h_f}{2}\dot{w}_b' - 2\dot{u}_c\right)\frac{2y^2}{h_c^2} + \left(\dot{u}_t - \dot{u}_b + \frac{h_f}{2}\dot{w}_t' + \frac{h_f}{2}\dot{w}_b' - h_c\dot{\phi}_1\right)\frac{4y^3}{h_c^3}\right)^2 + \left(\dot{w}_c + \frac{(\dot{w}_t + \dot{w}_b)y}{h_c} + \frac{(\dot{w}_t + \dot{w}_b - 2\dot{w}_c)2y^2}{h_c^2}\right)^2\right] dV_c \quad (2)$$

where ρ_f, ρ_c are the density of the face sheets, core of sandwich beam. The terms u_c ,u_t , u_b are longitudinal displacements at core, top and bottom face sheets and w_c ,w_t , w_b are vertical displacements at core, top and bottom face sheets and ϕ_1 is the slope at the centroid of the core. V_t , V_b , and V_c are the volume of the top face sheet, bottom face sheet, and core. The dots denote differentiation with respect to time (t) and the primes denote differentiation with respect to space (x). $\dot{u}_t$, $\dot{u}_b$, and $\dot{u}_c$ are the velocity of the top face sheet, bottom face sheet, and core in the longitudinal direction. $\dot{w}_t$, $\dot{w}_b$, and $\dot{w}_c$ are the velocity of top face sheet, bottom face sheet, and core in the transverse direction. $\dot{w}_t'$ and $\dot{w}_t'$, and $\dot{\phi}_1$ are the angular velocity of top face sheet, bottom face sheet, and core.

The kinetic energy of the tip mass is

$$T_{tip\, mass} = \frac{1}{2}M\left(\dot{w}_c(L,t) + \frac{L_M}{2}\dot{w}_c'(L,t)\right)^2 + \frac{1}{2}M\dot{u}_c^2 + \frac{1}{2}J_o\dot{w}_c'(L,t)^2 \quad (3)$$

where M is the mass of the payload, J_0 is the mass moment of inertia. $\dot{w}_c(L,t)$ and $\dot{w}_c'(L,t)$ are the velocity in the transverse direction and angular velocity of the centroid of the core at the end of the sandwich beam. $\dot{u}_c$ is the velocity in the longitudinal direction.

The kinetic energy due to the piezoelectric effect is given as

$$T_{piezo} = \frac{1}{2}\int \rho_a[(\dot{u}_t - y\dot{w}_t')^2 + \dot{w}_t^2]\, dV_a + \frac{1}{2}\int \rho_s[(\dot{u}_b - y\dot{w}_b')^2 + \dot{w}_b^2]\, dV_s \quad (4)$$

Where ρ_s and ρ_a are the density of the piezoelectric sensor and actuator attached to the sandwich beam. Here M is also the mass of tip mass. V_s and V_a are the volume of the piezoelectric sensor and actuator, respectively.

The potential energy of the beam is

$$U_{beam} = \frac{1}{2}\int_0^L \{ \int_{-\frac{h_f}{2}}^{\frac{h_f}{2}} E_f b\, (u_t' - yw_t'')^2 dy + \int_{-\frac{h_f}{2}}^{\frac{h_f}{2}} E_f b(u_b' - yw_b'')^2 dy + \int_{-\frac{h_c}{2}}^{\frac{h_c}{2}} E_c b\left(\frac{w_t - w_b}{h_c} + \frac{(w_t + w_b - 2w_c)4y}{h_c^2}\right)^2 dy + \int_{-\frac{h_c}{2}}^{\frac{h_c}{2}} G_c b[(\phi_1 - w_c') + (u_t + u_b + \frac{2h_f + h_c}{4}w_t' - \frac{2h_f + h_c}{4}w_b' - 2u_c)\frac{4y}{h_c^2} + (u_t - u_b + \frac{3h_f + h_c}{6}w_t' + \frac{3h_f + h_c}{6}w_b' - h_c\phi_1 - \frac{h_c}{3}w_c')\frac{12y^2}{h_c^3}]dy\}dx \quad (5)$$

Where E_f is the face sheets modulus of elasticity. E_c is the modulus of elasticity of the core. G_c is the shear modulus of the core.

The potential energy due to piezoelectric effect is given as

$$U_{piezo} = \frac{1}{2}\int_0^{L_p}\{\int_{\frac{h_f}{2}}^{\frac{h_f}{2}+h_a}\{E_a b(u_t' - yw_t'')^2 + 2e_{31}b\frac{\psi_a(x,t)}{h_a}(u_t' - yw_t'') - k_{33}b\left(\frac{\psi_a(x,t)}{h_a}\right)^2\}dy + \frac{1}{2}\int_{-\frac{h_f}{2}-h_a}^{-\frac{h_f}{2}}\{E_s b(u_b' - yw_b'')^2 + 2e_{31}b\frac{\psi_s(x,t)}{h_s}(u_b' - yw_b'') - k_{33}b\left(\frac{\psi_s(x,t)}{h_s}\right)^2\}dy\}dx \quad (6)$$

Where E_s, E_a are the modulus of elasticity of sensor and actuator, which are considered here the same as E_p. e_{31} is the piezoelectric coefficient, k_{33} is the dielectric coefficients. $\psi_a(x,t)$ and $\psi_s(x,t)$ are the unknown electric potentials at the mid-surface of the actuator and sensor.

The governing equations of motion are obtained using Hamilton's principle and are given by the following seven equations (Eqs.7-15):

$$m_f\ddot{u}_t + m_c\left[\frac{1}{20}(\ddot{u}_t + \ddot{u}_b) + \frac{1}{28}(\ddot{u}_t + \ddot{u}_b) + \frac{1}{15}\ddot{u}_c + \frac{1}{70}h_c\ddot{\phi}_1 + \frac{1}{40}h_f(\ddot{w}_t{}' - \ddot{w}_b{}') + \frac{1}{56}h_f(\ddot{w}_t{}' - \ddot{w}_b{}')\right] - E_f A_f u_t'' + \frac{G_c A_c}{h_c^2}\left[\frac{4}{3}(u_t + u_b) + \frac{9}{5}(u_t - u_b) - \frac{8}{3}u_c - \frac{4}{5}h_c\phi_1 + \left(\frac{2}{3}h_f + \frac{1}{3}h_c\right)(w_t' + w_b') + \left(\frac{9}{10}h_f + \frac{3}{10}h_c\right)(w_t' - w_b') + \frac{2}{5}h_c w_c'\right] - bh_a\left[E_p u_t'' - E_p\, h_m w_t''' + \frac{e_{31}\psi_a'}{h_a} + \rho_a\left(h_m\ddot{w}_t' - \ddot{u}_t\right)\right] = 0 \quad (7)$$

$$m_f \ddot{u}_b + m_c \left[\frac{1}{20}(\ddot{u}_t + \ddot{u}_b) - \frac{1}{28}(\ddot{u}_t + \ddot{u}_b) + \frac{1}{15}\ddot{u}_c - \frac{1}{70}h_c \ddot{\phi}_1 + \frac{1}{40}h_f(\ddot{w}_t{}' - \ddot{w}_b{}') - \frac{1}{56}h_f(\ddot{w}_t{}' - \ddot{w}_b{}')\right] - E_f A_f u_b'' + \frac{G_c A_c}{h_c^2}\left[\frac{4}{3}(u_t + u_b) - \frac{9}{5}(u_t - u_b) - \frac{8}{3}u_c + \frac{4}{5}h_c \phi_1 + \left(\frac{2}{3}h_f + \frac{1}{3}h_c\right)(w_t' + w_b') - \left(\frac{9}{10}h_f + \frac{3}{10}h_c\right)(w_t' - w_b') - \frac{2}{5}h_c w_c'\right] - bh_s\left[E_p u_b'' + E_p h_m w_b''' + \frac{e_{31}\psi_s'}{h_s} - \rho_s\left(h_m \ddot{w}_b' + \ddot{u}_b\right)\right] = 0 \tag{8}$$

$$m_c\left[\frac{8}{15}\ddot{w}_c + \frac{1}{15}(\ddot{w}_t + \ddot{w}_b)\right] + \frac{G_c A_c}{h_c^2}\left[-\frac{2}{5}u_t' - u_b' - \frac{4}{15}h_c^2 \phi_1 - \left(\frac{1}{5}h_f h_c + \frac{1}{5}h_c^2\right)(w_t'' + w_b'') - \frac{8}{15}h_c^2 w_c''\right] + \frac{E_c A_c}{h_c^2}\left[-\frac{8}{3}(w_t + w_b) + \frac{16}{3}w_c\right] = 0 \tag{9}$$

$$m_c\left[\frac{8}{15}\ddot{u}_c + \frac{1}{15}h_f^2(\ddot{u}_b + \ddot{u}_t) + \frac{1}{30}h_f(\ddot{w}_t' - \ddot{w}_b')\right] + \frac{G_c A_c}{h_c^2}\left[-\frac{8}{3}(u_t + u_b) + \frac{16}{3}u_c - \left(\frac{4}{3}h_f + \frac{2}{3}h_c\right)(w_t' - w_b')\right] = 0 \tag{10}$$

$$m_c\left[\frac{2}{105}h_c^2 \ddot{\phi}_1 + \frac{1}{70}h_c\,(\ddot{u}_t - \ddot{u}_b) + \frac{1}{140}h_f h_c(\ddot{w}_t' + \ddot{w}_b')\right] + \frac{G_c A_c}{h_c^2}\left[-\frac{8}{3}(u_t - u_b) + \frac{16}{3}u_c - \left(\frac{4}{3}h_f + \frac{2}{3}h_c\right)(w_t' - w_b')\right] = 0 \tag{11}$$

$$m_f\left(\ddot{w}_t - \frac{1}{12}h_f^2 \ddot{w}_t''\right) + m_c\left[-\frac{1}{40}h_f(\ddot{u}_t' + \ddot{u}_b') - \frac{1}{56}h_f(\ddot{u}_t' + \ddot{u}_b') - \frac{1}{30}h_f \ddot{u}_c' - \frac{1}{140}h_f h_c \ddot{\phi}_1{}' - \frac{1}{80}h_f^2(\ddot{w}_t'' + \ddot{w}_b'') + \frac{1}{12}(\ddot{w}_t - \ddot{w}_b) - \frac{1}{112}h_f^2(\ddot{w}_t'' + \ddot{w}_b'') + \frac{1}{20}(\ddot{w}_t + \ddot{w}_b) + \frac{1}{15}\ddot{w}_c\right] + E_f I_f w_t'''' + \frac{G_c A_c}{h_c^2}\left[-\left(\frac{2}{3}h_f + \frac{1}{3}h_c\right)(u_t' + u_b') - \left(\frac{9}{10}h_f + \frac{3}{10}h_c\right)(u_t' - u_b') + \left(\frac{4}{3}h_f + \frac{2}{3}h_c\right)u_c' + \left(\frac{2}{5}h_f h_c + \frac{2}{15}h_c^2\right)\phi_1' - \left(\frac{9}{20}h_f^2 + \frac{3}{10}h_f h_c + \frac{1}{20}h_c^2\right)(w_t'' + w_b'') - \left(\frac{1}{3}h_f h_c + \frac{1}{3}h_f^2 + \frac{1}{12}h_c^2\right)(w_t'' - w_b'') - \left(\frac{1}{5}h_f h_c + \frac{1}{15}h_c^2\right)w_c''\right] + \frac{E_c A_c}{h_c^2}\left[\frac{4}{3}(w_t + w_b) + (w_t - w_b) - \frac{8}{3}w_c\right] + bh_a\left[\rho_a(\ddot{w}_t) - E_p h_m u_t''' + E_p\left(\frac{h_f^2}{4} + \frac{h_f h_a}{2} + \frac{h_a^2}{3}\right)w_t'''' - e_{31}h_m\frac{\psi_a''}{h_a} + \rho_a h_m \ddot{u}_t' - \rho_a\left(\frac{h_f^2}{4} + \frac{h_f h_a}{2} + \frac{h_a^2}{3}\right)\ddot{w}_t''\right] = 0 \tag{12}$$

$$m_f\left(\ddot{w}_b - \frac{1}{2}h_f^2 \ddot{w}_b''\right) + m_c\left[-\frac{1}{40}h_f(\ddot{u}_t' + \ddot{u}_b') - \frac{1}{56}h_f(\ddot{u}_t' + \ddot{u}_b') + \frac{1}{30}h_f \ddot{u}_c' - \frac{1}{140}h_f h_c \ddot{\phi}_1{}' + \frac{1}{80}h_f^2(\ddot{w}_t'' + \ddot{w}_b'') - \frac{1}{12}(\ddot{w}_t - \ddot{w}_b) - \frac{1}{112}h_f^2(\ddot{w}_t'' + \ddot{w}_b'') + \frac{1}{20}(\ddot{w}_t + \ddot{w}_b) + \frac{1}{15}\ddot{w}_c\right] + E_f I_f w_b'''' + \frac{G_c A_c}{h_c^2}\left[\left(\frac{2}{3}h_f + \frac{1}{3}h_c\right)(u_t' + u_b') - \left(\frac{9}{10}h_f + \frac{3}{10}h_c\right)(u_t' - u_b') - \left(\frac{4}{3}h_f + \frac{2}{3}h_c\right)u_c' + \left(\frac{2}{5}h_f h_c + \frac{2}{15}h_c^2\right)\phi_1' - \left(\frac{9}{20}h_f^2 + \frac{3}{10}h_f h_c + \frac{1}{20}h_c^2\right)(w_t'' + w_b'') + \left(\frac{1}{3}h_f h_c + \frac{1}{3}h_f^2 + \frac{1}{12}h_c^2\right)(w_t'' - w_b'') - \left(\frac{1}{5}h_f h_c + \frac{1}{15}h_c^2\right)w_c''\right] + \frac{E_c A_c}{h_c^2}\left[\frac{4}{3}(w_t + w_b) + (w_t - w_b) - \frac{8}{3}w_c\right] + bh_s\left[\rho_s(\ddot{w}_b) + E_p h_m u_b''' + E_p\left(\frac{h_f^2}{4} + \frac{h_f h_a}{2} + \frac{h_a^2}{3}\right)w_b'''' + e_{31}h_m\frac{\psi_s''}{h_s} - \rho_s h_m \ddot{u}_b' - \rho_s\left(\frac{h_f^2}{4} + \frac{h_f h_a}{2} + \frac{h_a^2}{3}\right)\ddot{w}_b''\right] = 0 \tag{13}$$

$$e_{31}u_t' + h_m e_{31}w_t'' - \frac{k_{33}\psi_a}{h_a} = 0 \tag{14}$$

$$e_{31}u_b' + h_m e_{31}w_b'' - \frac{k_{33}\psi_s}{h_s} = 0 \tag{15}$$

Where h_m is defined as $\frac{h_f + h_a}{2}$ or $\frac{h_f + h_s}{2}$.

The boundary conditions are given by Eqs. (16)-(23) as

$$X = 0 \begin{cases} \delta u_t(0,t)\,, p_t(0,t) = 0 \\ \delta w_t(0,t)\,, V_t(0,t) = 0 \\ \delta w_t'(0,t)\,, M_t(0,t) = 0 \\ \delta w_c(0,t)\,, V_c(0,t) = 0 \\ \delta u_b(0,t)\,, p_b(0,t) = 0 \\ \delta w_b(0,t)\,, V_b(0,t) = 0 \\ \delta w_b'(0,t)\,, M_b(0,t) = 0 \end{cases}$$

$$
X = L \begin{cases} \delta u_t(L,t)\,, P_t(L,t) = 0 \\ \delta w_t(L,t)\,, V_t(L,t) = 0 \\ \delta w_t'(L,t)\,, M_t(L,t) = 0 \\ \delta w_c(L,t)\,, V_c(L,t) = 0 \\ \delta u_b(L,t)\,, P_b(L,t) = 0 \\ \delta w_b(L,t)\,, V_b(L,t) = 0 \\ \delta w_b'(L,t)\,, M_b(L,t) = 0 \end{cases} \tag{16}
$$

The general forms of the axial forces (P_t and P_b), the shear forces (V_t, V_b, V_c) and bending moments (M_t and M_b) are given as

$$
P_t = -E_f A_f \frac{\partial u_t}{\partial x} + bh_a \left\{ -E_p u_t' + E_p h_m w_t'' - \frac{e_{31}\psi_a}{h_a} \right\} - \left[\frac{M}{4} + \frac{ML_M^2}{4(h_f+h_c)^2} + \frac{J_0}{(h_f+h_c)^2} \right] \ddot{u}_t + \left[-\frac{M}{4} + \frac{ML_M^2}{4(h_f+h_c)^2} + \frac{J_0}{(h_f+h_c)^2} \right] \ddot{u}_b + \frac{ML_M}{2(h_f+h_c)} \ddot{w}_c \tag{17}
$$

$$
P_b = -E_f A_f \frac{\partial u_b}{\partial x} + bh_s \left\{ -E_p u_b' + E_p h_m w_b'' - \frac{e_{31}\psi_s}{h_a} \right\} + \left[-\frac{M}{4} + \frac{ML_M^2}{4(h_f+h_c)^2} + \frac{J_0}{(h_f+h_c)^2} \right] \ddot{u}_t - \left[\frac{M}{4} + \frac{ML_M^2}{4(h_f+h_c)^2} + \frac{J_0}{(h_f+h_c)^2} \right] \ddot{u}_b - \frac{ML_M}{2(h_f+h_c)} \ddot{w}_c \tag{18}
$$

$$
V_t = -\frac{1}{12} m_f h_f^2 \ddot{w}_t' + \frac{m_c}{840}\left(-36\, h_f \ddot{u}_t - 6 h_f \ddot{u}_b + 28 h_f \ddot{u}_c - 6 h_f h_c \ddot{\phi}_1 + 3\, h_f^2 \ddot{w}_b' - 18\, h_f^2 \ddot{w}_t'\right) + E_f I_f w_t'''' + \frac{G_c A_c}{840} h_c^2 \left[(196\, h_f - 28 h_c) u_b - (1316 h_f + 532\, h_c) u_t + (560 h_c + 1120 h_f) u_c + (28 h_c^2 - 98\, h_f^2 + 28\, h_f h_c) w_b'' - (112 h_c^2 + 658\, h_f^2 + 532\, h_f^2 + 532\, h_f h_c) w_t' + (336\, h_f h_c + 112 h_c^2)\phi_1 - (56 h_c^2 + 168\, h_f h_c) w_c' \right] + bh_a \left[\rho_a h_m \ddot{u}_t - E_p h_m u_t'' + E_p \left(\frac{h_f^2}{4} + \frac{h_f h_a}{2} + \frac{h_a^2}{3} \right) w_t''' - \rho_a \left(\frac{h_f^2}{4} + \frac{h_f h_a}{2} + \frac{h_a^2}{3} \right) \ddot{w}_t' - e_{31} h_m \frac{\psi_a'}{h_a} \right] \tag{19}
$$

$$
V_b = -\frac{1}{12} m_f h_f^2 \ddot{w}_b' + \frac{m_c}{840}\left(36\, h_f \ddot{u}_b + 6 h_f \ddot{u}_t + 28 h_f \ddot{u}_c - 6 h_f h_c \ddot{\phi}_1 + 3\, h_f^2 \ddot{w}_b' - 18\, h_f^2 \ddot{w}_t'\right) + E_f I_f w_b'''' + \frac{G_c A_c}{840} h_c^2 \left[(-196\, h_f + 28 h_c) u_t + (1316 h_f + 532\, h_c) u_b - (560 h_c + 1120 h_f) u_c + (28 h_c^2 - 98\, h_f^2 + 28\, h_f h_c) w_t'' - (112 h_c^2 + 658\, h_f^2 + 532\, h_f^2 + 532\, h_f h_c) w_b' + (336\, h_f h_c + 112 h_c^2)\phi_1 - (56 h_c^2 + 168\, h_f h_c) w_c' \right] + bh_s \left[-\rho_s h_m \ddot{u}_b + E_p h_m u_b'' + E_p \left(\frac{h_f^2}{4} + \frac{h_f h_s}{2} + \frac{h_s^2}{3} \right) w_b''' - \rho_s \left(\frac{h_f^2}{4} + \frac{h_f h_s}{2} + \frac{h_s^2}{3} \right) \ddot{w}_b' + e_{31} h_m \frac{\psi_s'}{h_s} \right] \tag{20}
$$

$$
V_c = \frac{G_c A_c}{840\, h_c^2} \left[-336 h_f (u_t - u_b) - 224 h_c^2 \phi_1 - (56 h_c^2 + 168\, h_f h_c)(w_t' - w_b') - 448 h_c^2 w_c' \right] - M \ddot{w}_c - \frac{ML_M}{2} \frac{\ddot{u}_b - \ddot{u}_t}{h_f + h_c} \tag{21}
$$

$$
M_t = -E_f I_f w_t{}'' + bh_a \left[E_p h_m u_t' - E_p \left(\frac{h_f^2}{4} + \frac{h_f h_a}{2} + \frac{h_a^2}{3} \right) w_t'' + e_{31} h_m \frac{\psi_a}{h_a} \right] \tag{22}
$$

$$
M_b = -E_f I_f w_b{}'' + bh_s \left[-E_p h_m u_b' - E_p \left(\frac{h_f^2}{4} + \frac{h_f h_s}{2} + \frac{h_s^2}{3} \right) w_b'' - e_{31} h_m \frac{\psi_s}{h_s} \right] \tag{23}
$$

Following [33], the direct velocity feedback control used here is given as

$$
\psi_a = G \dot{\psi}_s \tag{24}
$$

Where G is the velocity feedback gain.

NUMERICAL RESULTS AND DISCUSION

The numerical simulation is based on the material and geometric properties listed in Tables 1 and 2 for the sandwich beam with tip mass, and piezoelectric respectively. The first set of the numerical analyses is to validate the present formulation by comparing the obtained natural frequencies of the piezoelectric sandwich beam with tip mass using the GDQ method to those of Ansys simulation. The results are presented in Table 3 and show very good agreement. The results in Table 3 also indicate that the natural frequencies of sandwich beam-tip mass with piezoelectric patches are higher than those of the sandwich beam-tip mass without piezoelectric patches. This is expected as the presence of the piezoelectric patches make the sandwich beam stiffer.

Table 1: Material and geometric properties of the sandwich beam with tip mass

E_f (Gpa)	G_c (Mpa)	ρ_f $(\frac{kg}{m^3})$	ρ_c $(\frac{kg}{m^3})$	h_f (mm)
210	22.1	7900	60	1.9
h_c (mm)	L (mm)	b (mm)	ρ_M $(\frac{kg}{m^3})$	L_M (mm)
25	260	60	2600	70

Table 2: Material and geometric properties of piezoelectric PZT-4 [31]

E_a (Gpa)	E_s (Gpa)	$\rho_p(\frac{Kg}{m^3})$	$e_{31}(Cm^{-1})$
210	210	7500	-10
h_p (mm)	$L_p(mm)$	$b_p(mm)$	$K_{33}(10^{-9}Fm^{-1})$
0.25	52	60	10.275

Table 3: Natural frequency of sandwich beam-tip mass with and without piezoelectric patches

Case	GDQ	ANSYS
With piezoelectric patches	58.16 304.78 638.08	57.25 291.47 604.19
Without piezoelectric patches	57.91 304.14 637.77	56.92 289.67 601.62

The role of the piezoelectric patches location on the natural frequency of the system is illustrated in Table 4 using both GDQ and ANSYS simulation. It can be observed that the natural frequency decreases as the piezoelectric patches are placed farther from the clamp end. This is an indication that the sandwich beam is the stiffest when the piezoelectric is closer to the clamp end.

Table 5 depicts the effect of the piezoelectric patches length on the natural frequencies of the system. The results show that increasing the length of piezoelectric patches can increase or decrease the fundamental natural frequency of the sandwich beam with tip mass. For higher modes, it is observed that increasing the piezoelectric patches length consistently decreases the natural frequencies.

Table 4: Effect of piezoelectric patches location on the natural frequency (Hz) of sandwich beam-tip mass

Piezoelectric Location	$0 < X_p < 52$	$52 < X_p < 104$
GDQ	58.16 304.78 638.08	58.06 300.76 629.30
ANSYS	57.25 291.47 604.19	56.68 287.33 595.03

Table 5: Effect of piezoelectric patches length on the natural frequency (Hz) of sandwich beam-tip mass

Piezoelectric Length	$L_p = 52$	$L_p = 130$	$L_p = 260$
GDQ	58.16 304.78 638.08	58.24 298.47 629.29	58.07 294.06 619.40
ANSYS	57.25 291.47 604.19	57.30 286.39 594.29	56.84 279.07 580.99

The second part of the numerical simulation is to examine the piezoelectric vibration suppression of the sandwich bean with tip mass. The applied force is a rectangular pulse, which is defined as

$$F(t)\begin{cases} P & 0 < t < T \\ 0 & t > T \end{cases} \tag{25}$$

Here P is the magnitude of the load applied at the tip of the sandwich beam and T is the load duration. The value of P and T used in the numerical simulation are 10 N and 50 ms, respectively.

Figure 3 depicts the effect of the feedback control gain on the vibration response at the system (Fig. 3a) and voltage received by the actuator (Fig. 3b). The piezoelectric patches with length of 52 mm are attached near the clamped end at the top and bottom face sheets as depicted in Figure 1. The results in Fig. 3a indicate that the tip deflection of a sandwich beam decreases with increasing feedback gain. This figure also shows that increasing the feedback gain increases the actuator voltage.

The role of the location of the piezoelectric patches is depicted in Figure 4. For the specific example studied in this paper, the results in Fig. 4a indicate that superior vibration suppression can be achieved by attaching the piezoelectric patches closer to the tip mass.

(a)

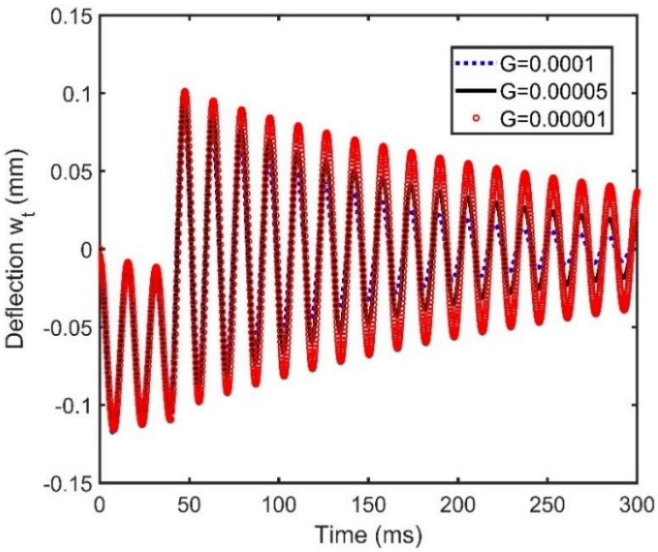

(b)

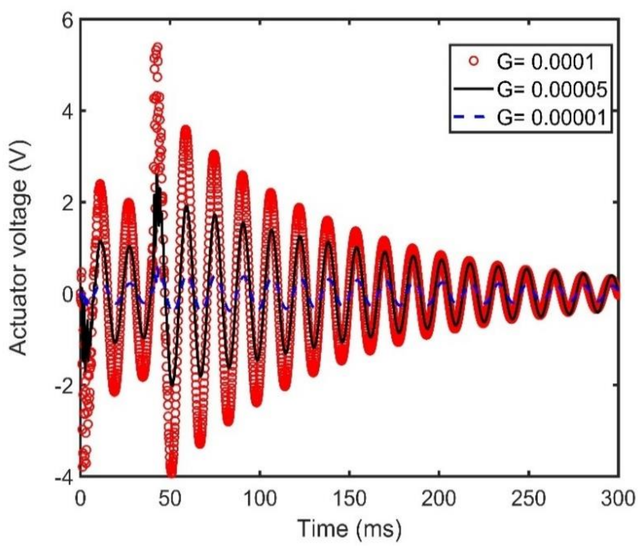

Figure 3: (a) Deflection of sandwich beam with tip mass (w_t), **(b)** Voltage receives by actuator with different feedback gain (G).

The least vibration performance is obtained when the piezoelectric patch is placed closer to the mid-point of the system. Fig. 4b also shows that highest transient actuator voltage is obtained when the piezoelectric patches are placed closer to the tip mass, but the highest steady state voltage is achieved when piezoelectric patches are placed near the middle of the sandwich beam-tip mass. These observations are a clear confirmation that the locations of the piezoelectric patches are crucial in controlling the vibration. It is anticipated that the best location of the piezoelectric patches should be closer to antinodes vibration loop. However, as this antinode varies with changing frequency, the best location of the piezoelectric patches should be obtained through optimization.

(a)

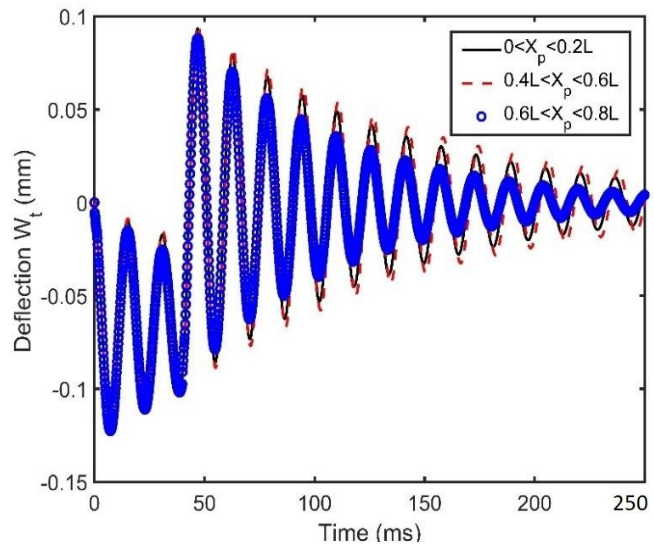

(b)

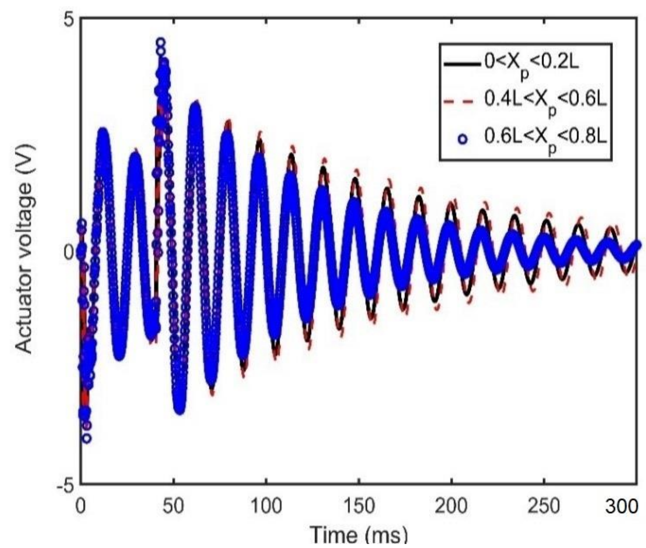

Figure 4: Role of location of piezoelectric patches: **(a)** Deflection of sandwich beam with tip mass (w_t), **(b)** Actuator voltage for a piezoelectric length of 52 mm and G=0.0001.

CONCLUSION

In this study, we presented for the first time the free and force vibration of a cantilever sandwich beam-tip mass with piezoelectric patches using higher-order sandwich panel theory. The equations of motion and boundary conditions were obtained using Hamilton's principle. Numerical analyses were conducted using the GDQ method to determine the natural frequencies and vibration response of the system. The results of the GDQ method were validated using Ansys simulation and showed very good agreement. Both Ansys and GDQ results showed that the natural frequencies of the sandwich beam-tip mass with piezoelectric patches are higher than those without piezoelectric patches. However, increasing the length of the piezoelectric, in general, decreases the natural frequencies of the system. This is due to the fact that the density of the piezoelectric in this case is more dominant than its stiffness. The natural frequencies of the system also increase as the piezoelectric patches were placed near the clamp end. Parametric studies were also conducted to analyze the role of the piezoelectric patches location on the vibration control of the sandwich beam-tip mass. It was observed that the location of piezoelectric patches is crucial in controlling the vibration of the system. The results related to presented model revealed that a best vibration control performance can be achieved when piezoelectric patches were attached near the tip mass. The worst performance was observed when they were placed closer to the middle of the sandwich beam. It should be noted, however, that these conclusions only pertain to the specific case presented in this paper. A more thorough study is needed to determine the optimum location of piezoelectric sensors and actuators for achieving best vibration control performance. The authors anticipate carrying out this task in their future work.

REFERENCES

[1] Liu, C., Jing, X., Daley, S., & Li, F., Recent advances in micro-vibration isolation. Mechanical Systems and Signal Processing, 56, 55-80. 2015.

[2] Yu, Y., Naganathan, N. G., Dukkipati, R.V., A literature review of automotive vehicle engine mounting systems. Mechanism and machine theory, 36(1), 123-142, 2001.

[3] Preumont, A., Vibration control of active structures: an introduction (Vol. 179). Springer Science & Business Media, 2011.

[4] Jalili, N., A comparative study and analysis of semi-active vibration-control systems. Transactions-american society of mechanical engineers journal of vibration and acoustics, 124(4), 593-605, 2002.

[5] Moita JMS., Correia VMF., Martins PG., Soares CMM, Soares CAM. Optimal design in vibration control of adaptive structures using a simulated annealing algorithm. Compos Struct;75(1–4): 79–87, 2006.

[6] Narayanan, S., Balamurugan, V., Finite element modeling of piezo laminated smart structures for active vibration control with distributed sensors and actuators. J Sound Vibration; 262(3):529–62, 2003.

[7] Liu G.R., Dai, K.Y., Lim, K.M., Static and vibration control of composite laminates integrated with piezoelectric sensors and actuators using the radial point interpolation method. Smart Mater Struct; 13(6):1438–47, 2004.

[8] Marinkovic D., Koppe H., Gabbert U., Accurate modeling of the electric field within piezoelectric layers for active composite structures. J Int Mat Syst Str; 18(5):503–13, 2007.

[9] Schmidt R., Vu TD., Nonlinear dynamic FE simulation of smart piezolaminated structures based on first- and third-order transverse shear deformation theory. Adv Mater Res;79–82: 2009.

[10] Valliappan. S., Qi, K., Finite element analysis of a 'smart' damper for seismic structural control. Comput Struct; 81(8–11):1009–17. 2003.

[11] Dong X.J., Meng G., Peng J.C., Vibration control of piezoelectric smart structures based on system identification technique: numerical simulation and experimental study. J Sound Vib;297 (3–5):680–93. 2006.

[12] Roy T., Chakraborty D., Optimal vibration control of smart fiber reinforced composite shell structures using improved genetic algorithm. J Sound Vib; 319(1–2):15–40. 2009

[13] Wang, Y., Inman, D.J., Energy-based comparison of various controllers for vibration suppression using piezoceramics, Active and Passive Smart Structures and Integrated Systems, San Diego, California, USA, 2011.

[14] Sadek, I.S., Kucuk , I., Adali, S., Active open-loop control of plates with multiple piezoelectric patches via the maximum principle, Mechanics of Advanced Materials and Structures, 21, 772–779, 2014.

[15] Chen C.Q., Shen Y.P., Optimal control of active structures with piezoelectric modal sensors andactuators. Smart Mater Struct ;6(4):403–9, 1997.

[16] Mohit, Chhabra, D., Kumar, S., Active vibration control of the smart plate using artificial neural network controller, Advances in Aerospace Engineering, 1–20, 2015.

[17] Zhang, X.-Y., Wang, R.-X., Zhang, S.-Q., Zhan, Wang Z-X, Qin, X.-S., Schmidt, R. Generalized-Disturbance Rejection Control for Vibration Suppression of Piezoelectric Laminated Flexible Structures. Shock and Vibration, 2018.

[18] Zhang, Q., Li, C., Zhang, J., Jin, J. Active Vibration Control and Coupled Vibration Analysis of a Parallel Manipulator with Multiple Flexible Links. Shock and Vibration. Volume 2016.

[19] Zippo, A., Ferrari, G., Amabili, M., Barbieri, M., Pellicano, F. Active vibration control of a composite sandwich plate. Composite Structures, 128, 100–114, 2015.

[20] Abdeljaber, O., Avci, O., Inman, D. Active vibration control of flexible cantilever plates using piezoelectric materials and artificial neural networks. Journal of Sound and Vibration 363, 33–53, 2016.

[21] Frostig, Y. and Baruch, M., Free vibrations of sandwich beams with a transversely flexible core: a high order approach. Journal of sound and vibration, vol. 176; 2, 195-208, 1994.

[22] Long R., Barry O. and Oguamanam DC. Finite element free vibration of soft-core sandwich beams. AIAA Journal; 50(1): 235-238, 2012.

[23] Frostig, Y. and Baruch, M., High-order buckling analysis of sandwich beams with transversely flexible core, Journal of Engineering Mechanics, vol. 119; 3, 476-492, 1993.

[24] Frostig, Y., Buckling of sandwich panels with a flexible core-high-order theory, "International Journal of Solids and Structures, vol. 35; 3-4, 183-204, 1998.

[25] Eshagh, F.J., Barry, O.R., Tanbour, H. E. Analytical and experimental vibration of sandwich beams having various boundary conditions, Shock and Vibration, 2018.

[26] Eshagh, F.J., Barry, O.R., Oguamanam, D.CD., Vibration of sandwich beams with tip mass: numerical and experimental investigations, Composite Structures *Submitted* (2018).

[27] Phan, C.N., Frostig, Y., Kardomateas, G.A., Blast response of a sandwich beam/wide plate based on the extended high-order sandwich panel theory and comparison with elasticity, Journal of Applied Mechanics, 80(6):061005, 2013.

[28] Trindade, M., Benjeddou, A., Ohayon, R. Piezoelectric active vibration control of a damped sandwich beams. Journal of Sound and vibration, 246(4), 653- 677, 2001.

[29] Malgaca, L. Integration of active vibration control methods with finite element models of smart laminated composite structures. Composite Structures 92, 1651–1663, 2010.

[30] Dafang, W., Liang, H., Bing, P., Wuewu, W., Shuang, W., Experimental study and numerical simulation of active vibration control of a highly flexible beam using piezoelectric intelligent material. Aerospace Science and Technology 37, 10–19, 2014.

[31] Shunqi, Z., Schmidt, R., Xiansheng, Q. Active vibration control of piezoelectric bonded smart structures using PID algorithm. Chinese Journal of Aeronautics, 28(1): 305–313, 2015.

[32] Trindade, M., Hybrid active-passive damping treatements using viscoelastic and piezoelectric materials: Review and assessment. Journal of Vibration and Control, 8: 699–745, 2002.

[33] Bodaghi, M., Damanpack, A.R., Aghdam, M.M., Shakeri, M., Non-linear active control of FG beams in thermal environments subjected to blast loads with integrated FGP sensor/actuator layers: Composite Structures, 3612-3623, 2012.